Journal of Cleaner Production 568 (2026) 148694

Contents lists available at ScienceDirect

Journal of Cleaner Production

journal homepage: www.elsevier.com/locate/jclepro

Impact of polysaccharides, proteins, lipids, and humic-like substances on thermal stability and flammability of wastewater sludge extracellular polymeric substances

Tan Minh Le [a,b], Yuemei Lin [c], Wei-Qin Zhuang [d], Mark C.M. van Loosdrecht [c], Krishnan Jayaraman [a,b], Nam Kyeun Kim [a,b,*]

[a] Centre for Advanced Materials Manufacturing and Design, University of Auckland, Auckland, 1023, New Zealand
[b] Department of Mechanical and Mechatronics Engineering, University of Auckland, Auckland, 1010, New Zealand
[c] Department of Biotechnology, Delft University of Technology, Delft, 2629HZ, the Netherlands
[d] Department of Civil and Environmental Engineering, University of Auckland, Auckland, 1010, New Zealand

HIGHLIGHTS

- Thermal decomposition and flammability of EPS are studied by their individual components.
- The pyrolysis mechanisms are explored using TG-FTIR combined with 2DCOS.
- Polysaccharides show higher char-forming ability than other components.
- Protein and humic-like substances are main contributors to emit non-volatile gases.
- Lipids drive flammability of EPS through CH_4 release and poor charring capacity.

GRAPHICAL ABSTRACT

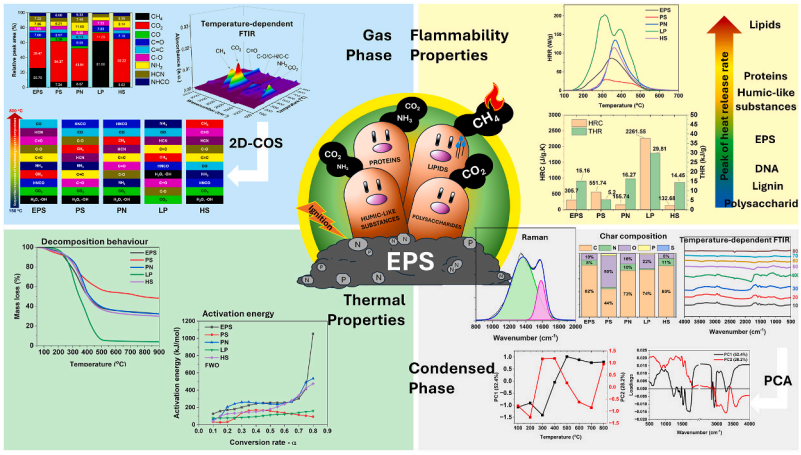

ARTICLE INFO

Keywords:
Extracellular polymeric substances
Biopolymers
Activated sludge
Flammability
Thermal decomposition

ABSTRACT

The current study investigates the application of extracellular polymeric substances (EPS), recovered from municipal wastewater sludge, as sustainable flame-retardant materials. While EPS show significant fire-safety potential, their compositional complexity requires a clear understanding of fire performance. The primary objective of this research is to elucidate how key EPS components, such as proteins (PN), polysaccharides (PS), lipids (LP), and humic-like substances (HS), govern thermal decomposition and flammability. Thermogravimetric analysis reveals that PN and HS have higher activation energies than those of other components, enhancing EPS thermal stability. PS yield the highest char residue (48.7% at 900 °C), while PN achieve the highest

* Corresponding author. Centre for Advanced Materials Manufacturing and Design, University of Auckland, B903, 262 Khyber Pass Road, Auckland, 1023, New Zealand.
E-mail address: nam.kim@auckland.ac.nz (N.K. Kim).

https://doi.org/10.1016/j.jclepro.2026.148694
Received 18 December 2025; Received in revised form 17 May 2026; Accepted 3 June 2026
Available online 8 June 2026

graphitisation degree, highlighting their crucial roles in char formation of EPS. Pyrolysis gas analysis indicates that PN and HS are main sources of nitrogenous compounds, diluting oxygen. Moreover, flammability tests show PS have the lowest peak heat release rate (29.7 W/g), underlining the important role in increasing flame-retardancy of EPS. However, TGA-FTIR analysis indicates lipid as a primary source of combustible gases likely due to their hydrocarbon chains. This study provides valuable insight into the role of major EPS components in the flame-retardant properties and suggest a sustainable approach to enhance flame retardancy through targeted component optimisation.

1. Introduction

Extracellular polymeric substances (EPS) are a main organic fraction of activated sludge, a by-product of wastewater treatment plants (WWTPs) (Hamed et al., 2025). Since extracellular polymeric substances (EPS) govern water retention in sludge matrices, their extraction improves sludge dewaterability and drying performance, thereby facilitating sludge volume reduction. EPS recovery also offers an economically viable pathway by reducing costly waste disposal volumes while simultaneously generating high-value, marketable bio-products, thus aligning with circular economy principles (Zheng et al., 2024). In the Netherlands specifically, EPS recovery is projected to reach several hundred tonnes annually, creating an estimated €170 million in value by 2030 (van Leeuwen et al., 2018). EPS exhibit valuable functionalities, such as metal-binding capacity, amphiphilicity, and gelling behaviour, rarely found in other materials (Zheng et al., 2024). Recently, EPS have been discovered as a novel flame retardant on flax fabric (Kim et al., 2020) and linen fabric (C. Li et al., 2024) as EPS coating significantly reduces the heat release rate of these fabrics. Therefore, the development of EPS as a flame retardant not only addresses the waste management issues of WWTPs but also provides a novel bio-flame retardant for the materials industry since synthetic flame retardants, especially halogenated additives, have been banned by many countries.

Different from some conventional bio-flame retardants (e.g. lignin, phytic acid, etc), EPS are composed of various components, such as polysaccharides (PS), proteins (PN), humic-like substances (HS) and lipids (LP). Among these, PS and PN are the main components, accounting for 40 – 95 % and 10 – 60 % of EPS, respectively. HS, LP, and other components make up 1 -20% of EPS (Tang et al., 2020). Although many studies have claimed that PS and PN take the main responsibility for the properties of EPS (e.g. gelling properties)(Yu et al., 2020, 2023), for flame-retardant properties, all components collectively contribute and interact during combustion, influencing the overall flame-retardant performance of EPS. In fact, these individual components have been used to develop flame-retardant materials (Jeong et al., 2022; Venezia et al., 2023). For example, casein, a milk protein containing phosphorus, can be used as a flame retardant in wood fibreboards as it can create a char and release phosphorus-containing compounds against the fire (Lee et al., 2024). showed that the phosphorylated casein can reduce the peak heat release rate (pHRR) of wood fibreboard by 18%. Further, Wang et al. (Zhao et al., 2015) demonstrated that modified cardanol, a phenolic lipid in cashew nutshell, can decrease the pHRR of epoxy by 20% when incorporated in epoxy. According to Kim et al. (2022), the presence of phosphorus in EPS can promote the char formation and protect the underlying materials against the heat. Although flame-retardant potential of the biopolymers is reported, their specific contributions to the thermal stability and flame retardancy of EPS remain largely unexplored.

Understanding the role of individual EPS components in flame-retardant performance is a critical step in the development of EPS-based flame retardants. For instance, the well-known intumescent flame-retardant system comprises dehydration agents (e.g. amide phosphate, alkyl phosphates, sulphate salts, etc.), carbon-rich sources (e.g. cellulose, starch, etc.), and blowing agents (e.g. melamine, urea, etc.) (Enescu et al., 2013). Each component plays an important role in forming char which can act as a barrier to reduce material's flammability. In fact, EPS also contain the required components for the intumescent flame-retardant system. Theoretically, the phospholipid can be seen as a dehydration agent due to its alkyl phosphate structure. PS and HS are carbon-rich sources, while PN can act as a blowing agent. Moreover, the differences in the characteristics of PS, PN, HS and LP can significantly affect the properties of EPS. Recently, it has been discovered that despite using various extraction methods, the thermal stability of EPS is mainly affected by the contents of PS, PN, HS and LP, but PN and HS play a prominent role in enhancing their thermal properties (Minh Le et al., 2025). When studying the flame-retardant mechanism of EPS, it was also found that the PS, PN, HS and LP always contribute to the gaseous products during the EPS combustion (Minh Le et al., 2025). This finding suggests that these components can play important roles in the flame-retardant properties of EPS. Based on the available literature, no prior study has specifically investigated the fire performance of individual components within EPS.

This study aimed to understand the thermal properties and flammability of EPS components and their potential contribution to the flame-retardant properties of EPS. First, PS, PN, LP, and HS were separately extracted from EPS generated from activated sludge. It is known that the flame-retardant properties of EPS were defined by their thermal properties, char formation, heat released, and the gas released during the decomposition (Kim et al., 2023; Le et al., 2025). To assess these factors, the thermal decomposition profiles of EPS components were investigated using thermogravimetric analysis (TGA) to estimate activation energy (AE). The char structure and composition of each component were determined by using Raman spectroscopy, and Energy Dispersive X-ray Spectroscopy (EDS). The temperature-dependent FTIR spectra integrating with principal component analysis (PCA) were used to monitor functional group evolution during the char formation. The fire reaction properties of EPS components were measured by micro-combustion calorimeters (MCC) to generate data related to heat release during the combustion. The gases released during the pyrolysis of each EPS component were analysed using TGA-FTIR to elucidate the flame-retardant mechanisms occurring in the gas phase. In addition, two-dimensional correlation spectroscopy (2D-COS) was applied to the FTIR spectra of the gas phase to gain insight into the thermal decomposition behaviour of these EPS components. Finally, based on the experimental findings, the contributions of PS, PN, LP, and HS to the flame-retardant behaviour of EPS are discussed.

2. Materials and methods

The materials and methods in this study are detailed in the supplementary information. The summarised approaches used in this study are shown in Fig. 1.

2.1. Materials

Activated sludge was collected from Māngere wastewater treatment in Auckland, New Zealand. EPS were extracted following the sodium hydroxide and heating method (Le et al., 2025). The main EPS components—polysaccharides (PS), proteins (PN), lipids (LP), and humic-like substances (HS)—were subsequently separated based on established protocols in the literature.

Lipids were first extracted using a chloroform: methanol mixture (2:1

v/v) following Wang et al. (2017) to minimise interference with the separation of other components. The extraction was performed at 30–35 °C with a solid-to-liquid ratio of 1:25 g/mL, involving two extraction cycles (12 h and 5 h). After two cycles, the mixture was filtered under vacuum, and the solid EPS residue was washed with water and dried at 50 °C. The combined lipid-solvent extracts were evaporated at 35 °C using a vacuum rotary evaporator to obtain LP. Then, the EPS after lipid extraction were dissolved in NaOH 0.1 M at concentrations of 10 g/L. The polysaccharides (PS) were isolated via ethanol precipitation (Wei et al., 2019).

Proteins (PN) extracted using the three-phase partitioning (TPP) method (Antunes et al., 2024; Qiu et al., 2024) because of its simplicity and high selectivity for protein. The extraction condition was chosen based on the previous studies and our preliminary results. Briefly, 30 g of $(NH_4)_2SO_4$ was gradually added to 100 mL of EPS solution (10 g/L) in NaOH 1w/v% at 35 °C with stirring at 300 rpm. Then, 100 mL of t-butanol was added, and the mixture was allowed to settle for 30 min, forming three distinct layers. The protein-rich middle layer (Fig. S1) was collected by centrifugation, rinsed with deionised water, and dried at 50 °C.

Humic-like substances were isolated from EPS following the protocol of the Humic Substances Society (Aiken et al., 1986; Yuan et al., 2022). The EPS solution in NaOH 1w/v% was initially acidified with HCl 5 M to pH 2 under a nitrogen atmosphere. The mixture was incubated for 12 h. Next, the obtained precipitation was collected and rinsed several times with DI water. All the experiments were repeated at least three times with the same EPS.

2.2. Thermal properties and flammability properties characterisation

2.2.1. Thermal properties

The thermal degradation profiles of EPS and their components were measured using a thermogravimetric analyser (TA Q5000, TA instruments, USA) at different heating rates (10, 30 and 60 °C/min), 50 – 900 °C, under a nitrogen atmosphere with a flow rate of 50 mL/min. The experiments were replicated to ensure the accuracy and reproducibility of data. The activation energy (AE), was estimated using Flynn–Wall–Ozawa (FWO) and Kissinger-Akahira-Sunose (KAS) methods, as expressed:

$$\text{FWO equation}: \ln\beta = c - 1.052\frac{E}{RT} \quad (1)$$

$$\text{KAS equation}: \ln\left(\frac{\beta}{T^2}\right) = \ln\left(\frac{AR}{Eg(\alpha)}\right) - \frac{E}{RT} \quad (2)$$

where β is the heating rate (°C/min), c is a constant, E is activation energy (kJ/mol), R is the ideal gas constant (8.314 J/mol·K), and T is the absolute temperature (K). and g(α) is a function of the conversion rate (α). A is the pre-exponential factor. α is the reaction rate calculated as

$$\alpha = \frac{W_o - W_i}{W_o - W_f} \quad (3)$$

where W_i, W_o, and W_f (mg) are the weights of the sample at time i, initial, and final, respectively.

2.2.2. Flammability properties

Micro-combustion calorimeter (MCC - FAA Micro Calorimeter, FTT, UK) were used to evaluate the flammability of EPS and their components following ASTM D7309 (Schinazi et al., 2022). The samples were subjected to a pyrolyser in a nitrogen atmosphere and then heated to 700 °C at 60 °C/min (1 K/s). The volatile released from the pyrolyser were swept to a combustor, where they were burnt in simulated air (O_2: N_2 = 20:80) at 900 °C. The amount of oxygen consumption was recorded to calculate the heat release rate (HRR), total heat release (THR), and heat release capacity (HRC).

2.3. Gas and char analysis methods

2.3.1. Pyrolytic gas analysis

The volatile gases released during the pyrolysis of EPS and each component, depending on the temperature, was monitored using TG-

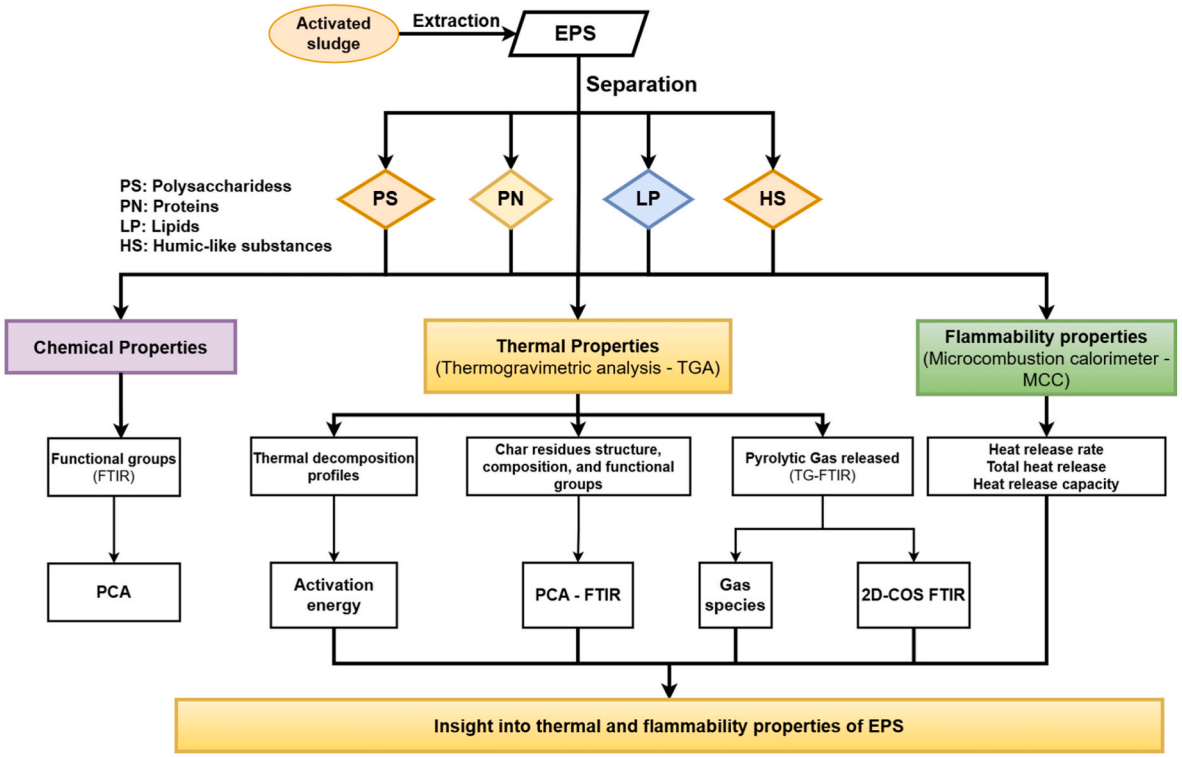

Fig. 1. Schematic diagram showing approaches used in this study. PCA – principal component analysis, 2D-COS – two-dimensional correlation of spectroscopy.

FTIR (Perseus, alpha II FT-IR, Bruker, Australia) with a wavenumber range of 4000 – 400 cm^{-1} every 15 s for each sample. The heating rate was selected at 60 °C/min to compare with MCC results. The interface transfer line was kept at 200 °C to prevent condensation of gaseous products.

2.3.2. Char residue characteristics

The char residues from TG testing at different temperatures were collected to determine the char formation of EPS and their components using FTIR (Nicolet iS50 FTIR Spectrometer, Thermo Fisher Scientific, USA) with a wavenumber range of 4000-400 cm^{-1}. The char residues at 700 °C were determined graphitisation degree using the Raman spectroscopy (Horiba Jobin-Yvon, Japan) and elemental content using Energy-dispersive spectroscopy (EDS) detector (Oxford Instruments, UK).

2.4. Gas and char analysis methods

2.4.1. Pyrolytic gas analysis

The volatile gases released during the pyrolysis of EPS and each component, depending on the temperature, was monitored using TG-FTIR (Perseus, alpha II FT-IR, Bruker, Australia) with a wavenumber range of 4000 – 400 cm^{-1} every 15 s for each sample. The heating rate was selected at 60 °C/min to compare with MCC results. The interface transfer line was kept at 200 °C to prevent condensation of gaseous products.

2.4.2. Char residue characteristics

The char residues from TG testing at different temperatures were collected to determine the char formation of EPS and their components using FTIR (Nicolet iS50 FTIR Spectrometer, Thermo Fisher Scientific, USA) with a wavenumber range of 4000-400 cm^{-1}. The char residues at 700 °C were determined graphitisation degree using the Raman spectroscopy (Horiba Jobin-Yvon, Japan) and elemental content using Energy-dispersive spectroscopy (EDS) detector (Oxford Instruments, UK).

2.5. Data analysis

2.5.1. Principal component analysis (PCA)

PCA is a multivariate statistical technique for analysing large data by transforming the original variables into new uncorrelated variables, named principal components (PC). PCA was used to visualise the changes in FTIR spectra of EPS components at various temperatures and distinguish the FTIR spectra between these components. Before analysis, the FTIR was normalised and baseline corrected to reduce the effects of noise. The number of principal components was selected based on the criteria of eigenvalues greater than 1 and a percentage of cumulative explained variance greater than 80%. In this study, the PCA was performed using OriginPlab 2025 software.

2.5.2. Two-dimensional correlation of spectroscopy (2D-COS)

In this study, the 2D-COS analysis was used to improve the readability of FITR spectra changes by temperature and to understand the response of EPS and their components to temperature. The changes of spectra variables (x) based on different external perturbations of temperature (T) functioned as A(x,T) (Lasch and Noda, 2019). The population of a series of m spectrums by the different perturbations was denoted as a dynamic spectrum - $\widetilde{A}(x,T)$.

$$\widetilde{A}(x_k,T_i)=\begin{cases} A(x_k,T_i)-\overline{A}(x_k), for\ 1\le i\le m \\ 0\ otherwise \end{cases} \quad (4)$$

Where $\overline{A}(x_k)$ was the average spectrum.

Fundamentally, 2D-COS analysis is conducted based on two signals of synchronous and asynchronous correlation spectra, which are computed as follows:

$$\text{Synchronous}: \phi(x_1,x_2)=\frac{1}{m-1}\sum_{i=1}^{m}\widetilde{A}(x_1,T_i)\cdot\widetilde{A}(x_2,T_i) \quad (5)$$

$$\text{Asynchronous}: \psi(x_1,x_2)=\frac{1}{m-1}\sum_{i=1}^{m}\widetilde{A}(x_1,T_i)\cdot\sum_{j=1}^{m}N_{ij}\widetilde{A}(x_2,T_j) \quad (6)$$

Where: $N_{i,j}=\begin{cases} 0\ \ for\ i=j \\ \dfrac{1}{\pi(j-i)}\ for\ otherwise \end{cases}$ is an element of the Hilbert-Noda transformation matrix (Noda et al., 2000).

In the synchronous spectra, the autocorrelation peak in the diagonal position suggests the sensitivity of corresponding function groups to the temperature. The cross-peak outside of the diagonal implies the changing direction of two spectral variables. For instance, if ϕ (x_1,x_2) is positive, x_1 and x_2 have the same direction of change.

The asynchronous spectra point out the order changes of the two variables. According to Noda's rules (Noda et al., 2000), if synchronous - $\phi(x_1,x_2)$ and asynchronous - $\psi(x_1,x_2)$ spectra have a same sign, the x_1 changes before x_2, else x_1 changes after x_2. In this work, the 2D-COS analysis was conducted using the 2D correlation function on Originlab software (Originlab, USA) in the temperature range of 150 – 800 °C.

2.5.3. Statistical analysis

In this study, one-way analysis of variance (ANOVA) was used to analyse single-factor experiments, followed by the Least Significant Difference (LSD) post hoc test. Statistical significance was determined at an alpha level of 0.05 ($p < 0.05$). All analyses were performed using SPSS (IBM, USA). For multiple comparisons among groups, Tukey's post hoc test was also applied to assess pairwise differences. The data analysis was carried out using SPSS (IBM, USA).

3. Results and discussion

3.1. Thermal properties of EPS components

3.1.1. Thermal decomposition profiles of EPS components

The thermal decomposition behaviour of EPS components is reported in Table 1 and Fig. 2. The pyrolysis behaviour of materials has strong correlations with their chemical structures (Zong et al., 2020). As shown in Fig. 2a, LP decompose between 150 °C and 550 °C with two DTG peaks at 308 °C and 396 °C, indicating the presence of two LP types. The first peak corresponds to the breakdown of short-chain fatty acid esters, such as acetic, propionic, and butyric acids (Tain et al., 2021), while the second is attributed to the degradation of long-chain aliphatic structures. Unlike palm-derived lipids, which typically leave no char at 900 °C, as reported by Zong et al. (2020), LP from EPS produced 3.9% char residue, likely due to Diels–Alder condensation reactions facilitated by their aliphatic structure (Yang et al., 2019).

PS decompose between 227 °C and 585 °C with a maximum decomposition rate of 14.16 %/min at 307 °C. Their lower decomposition temperature, compared to PN and HS, is attributed to the abundance of 1,4-glycosidic linkages align the glucose units so that numerous inter- and intrachain hydrogen bonds form primarily between hydroxyl groups, which are easier to decompose (Zhang et al., 2021). PS, e.g. cellulose and starch, have been known as a group of compounds that generate low char residues (often less than 10%) (Zong et al., 2020). However, in this study, PS generated the highest char residue amount of 48.3 % at 900 °C compared to other samples. These different results are due to the complicated structure of PS in EPS. During the wastewater treatment, under the biological activity of bacteria, cell lysis, and their interaction with other components, many derivatives of PS may occur. For example, Li et al. (J. Li et al., 2024) recently reported the existence of lipopolysaccharides – a phosphorus-containing polysaccharide-in the

Table 1
TGA data of EPS and their components at heating rates of 60 °C/min.

Parameters	Polysaccharides	Proteins	Lipids	Humic-like substances	EPS
T_{in} (°C)	227 °C$^{\alpha}$	205 °C$^{\beta}$	150 °C$^{\zeta}$	220 °C$^{\delta}$	175 °C$^{\varepsilon}$
T_{max1} (°C)	307	267	308	264[a]	250[a]
R_{max1} (%/min)	14.16	6.27[a]	30.05	9.54[a]	11.84[a]
T_{max2} (°C)	728	381	396	363	347
R_{max2} (%/min)	2.02	24.11	22.57	24.93	18.61
Char yield at 900 °C (%)	48.16 ± 0.067$^{\alpha}$	32.30 ± 2.91$^{\beta}$	3.91 ± 0.05$^{\zeta}$	29.91 ± 1.5δ	32.1 ± 2.83$^{\varepsilon}$

The different superscript symbols in same row imply significant difference between values ($p < 0.05$).
[a] shoulder peak.

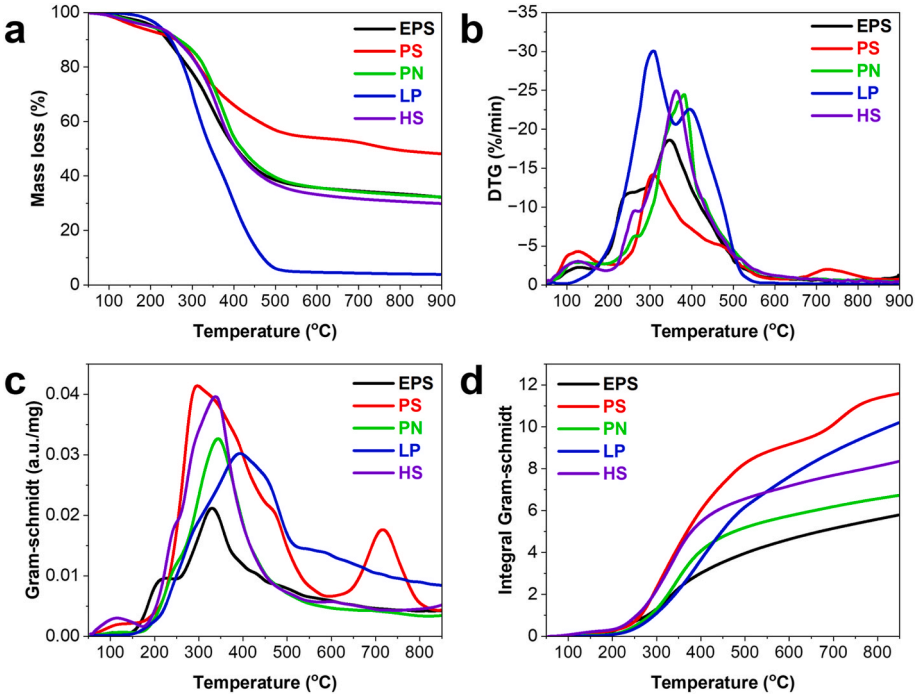

Fig. 2. TGA (a), DTG (b), Gram-Schmidt (c) and its integral (d) curves of EPS and their isolated components at a heating rate of 60 °C/min.

EPS extracted from activated sludge. Wang et al. (Wang et al., 2017) suggested that the lipopolysaccharides in microalgae-derived PS are also the reason for their high char residues (35.57 %). The underlying mechanism of the high char residues can be attributed to the presence of phosphorus in the PS structure, which can catalyse the carbonisation process (Sun et al., 2024). In addition, certain types of PS can also create high char residues (more than 10%), like hemicellulose and chitin (Liu et al., 2020). demonstrated that hemicellulose, isolated from sesame hulls using the ethanol precipitation method, can produce 45% char residues at 600 °C. Hemicellulose is constituted by xylan, containing pentoses and hexose sugars, which makes it easier to form a char compared to cellulose (Stefanidis et al., 2014). Chitin – a nitrogen-containing polysaccharide, can also produce 21% of char residues at 800 °C due to the reinforcement of N element in its structure (Liu et al., 2023). Therefore, to better understand the structure and properties of char generated from PS, further analyses are also conducted and discussed in Section 3.2.

Interestingly, the TGA and DTG curves of PN and HS are quite similar. The decomposition ranges of PN are 205 – 620 °C, while those of HS are 220 – 700 °C. HS are composed of various functional groups, such as quinone, phenol, carboxyl and hydroxyl groups (Venezia et al., 2023), which mainly contain aromatic structures (Wang et al., 2023). In the wastewater treatment process, the HS are formed by the degradation of protein-like substances (Dai et al., 2013) and organic matter (Michalska et al., 2022) under the bioactivity of microorganisms in the sludge. PN are mainly composed of amino acids, including both aliphatic amino acids and aromatic amino acids, such as glutamic acid and phenylalanine. Therefore, most likely, some of the aromatic structures in PN can contribute to the formation of HS, leading to similar thermal decomposition of both components. In addition, because of the high aromatic structure, both PN and HS exhibit higher char residues at 900 °C than LP, with values of 32.30% and 29.91%, respectively.

The decomposition temperature of EPS ranges from 175 °C to 600 °C, with one DTG shoulder at 250 °C and one main peak at 347 °C. In general, without any synergistic and antagonistic interaction of these components, the TGA and DTG curves of EPS should be expected to represent an average value of their components. Obviously, in the temperature range of 175 – 300 °C, the decomposition rate of EPS and its components are in the sequence of PS < PN < HS < EPS < LP. The higher decomposition rate of LP than other components indicate the stronger effects of LP on the pyrolysis behaviour of EPS in this stage. When the temperature is increased from 300 to 600 °C, the DTG values of these samples are in the order of LP > EPS > PS > PN > HS.

The total amounts of gas released during the decomposition of EPS components are monitored through Gram-Schmidt and its integral curves (Fig. 2c–d). Gram-Schmidt is a function of the total absorbance of gaseous products with temperature. For comparison purposes, the Gram-Schmidt was normalised with sample weight and integrated, as depicted in Fig. 2c–d. Both PS and HS exhibit a small peak at around 100 °C due to the de-hydroxyl groups of these compounds. The total gas

absorbance of the EPS components is in the order of EPS < PN < HS < LP < PS, suggesting that EPS releases the least amount of gaseous products among the studied compounds. Surprisingly, the PS released the highest amount of gaseous products compared to others, suggesting their strong devolatilisation reaction. From 300 to 800 °C, the amount of gas released from LP is significantly increased, indicating that the cracking of long-chain fatty acids can promote the release of gaseous products. HS emit more gaseous products than PN, which can be attributed to the complicated chemical structure of HS, potentially containing various thermally unstable compounds. Notably, EPS have the lowest gas release from 300 to 800 °C, proposing that the interaction between these components can contribute to reducing the gas release during EPS decomposition.

3.1.2. Activation energy

TG and DTG curves mainly provide information related to the weight loss and decomposition rate. In order to investigate thermal stability more deeply, the activation energy of pyrolysis reactions of samples is calculated using TG/DTG data, as shown in Fig. 3.

Different heating rates from 150 to 700 °C are selected to obtain AE values of all samples since this is the main decomposition temperature of these samples, as illustrated in Figs. S2–S6. In each sample, the shape of DTG curves at different heating rates is similar, supporting that the pyrolysis reaction mechanisms are not influenced by the heating rate (Figs. S2–S6). The AE values of PS are the lowest at conversion rates of 0.1 to 0.2 because of the decomposition of hydroxyl groups and the breaking of β-1,4-glyscosidic bond in hemicellulose structure at temperatures of 150 – 250 °C (Chen et al., 2020a). Their AE values significantly increase from α = 0.2 to 0.4 and reach a peak of 170 kJ/mol at α = 0.4. This is due to the formation of mediate products, as active cellulose in the case of cellulose (Anca-Couce, 2016), which requires high energy. Afterwards, the AE values gradually decrease to 93 kJ/mol at α = 0.8, which may be attributed to the rearrangement of the carbon structure catalysed by phosphorus. Cabrera-Barjas et al. (2023) reported that increasing phosphorus content in phosphorylated chitin—a N-containing polysaccharide—not only promotes char formation but also reduces the activation energy compared to pure chitin. The AE values of PN increase with α, ranging from 0.1 to 0.35, due to the cleavage of the unstable bonds in the PN structure. For α ranging from 0.35 to 0.65, the AE of PN is unchanged as the deamination, dehydration, and decarboxylation reactions happen, leading to the release of N-containing compounds, such as pyridine, pyrrole, indole and other heterocyclic nitrogen (Wang et al., 2017). From 0.6 to 0.8, the AE values of PN show a rapid increase from 245.61 to 536.06 kJ/mol, due to the condensation reaction (Zong et al., 2020).

LP, composed mainly of glycerol and fatty acids, display nearly constant AE values due to their simple molecular structure and straightforward bond cleavage during pyrolysis. LP exhibits the lowest AE value among the components, indicating that its structure is less favourable for improving the thermal properties of EPS. The slight increase in AE from α = 0.6 suggests that the Diels-Alder reaction of alkenes into a cyclo-structure, as demonstrated by the small residue remaining after the pyrolysis. The changes in AE values of HS during the decomposition process can be divided into three stages. In the first stage, from α = 0.1 – 0.3, the AE values of HS increased from 40.70 to 140.34 kJ/mol for the FWO method, due to the decomposition of short molecular chains (Zong et al., 2020). The second stage, from 0.4 to 0.6, is associated with the thermal degradation of long molecular chains. The final stage is related to the decomposition of aromatic structures and their cross-linking reaction to form a char structure.

In comparison, the AE of EPS is higher than all components at the conversion rates of 0.1 – 0.15, suggesting that the interaction of these compounds can contribute to the enhanced thermal stability of EPS. In the elevated conversion rates, the AE values of EPS are increasing, from 171.70 to 1054.10 kJ/mol, implying the formation of thermally stable products of EPS. The average AE values of these samples are in sequence with EPS > PN > HS > PS > LP, suggesting the potential of collective effects of these components.

3.2. Investigation on the char formation of EPS components

3.2.1. Char composition and structure

The char residues at 700 °C from PS, PN, LP, and HS are evaluated using EDS and Raman spectroscopy, as shown in Table 2. The elemental analysis by EDS depicts that the carbon content in the char residues of all samples ranges from 44 to 82%. Notably, the phosphorus content in the char of PS is the highest (2.90 %) among the components, followed by LP's char (1.89 %). As mentioned, the phosphorus in PS can come from the lipopolysaccharides, which is verified by Li et al. (J. Li et al., 2024). The phosphorus in LP's char residue is from phospholipid, a main structural component in the cell wall of microorganisms in the sludge matrix. Nevertheless, the overall phosphorus content in EPS char remains low (0.68%) due to the minor abundance of these phosphorus-bearing compounds. On the other hand, PN and HS are primary nitrogen sources of EPS, where 10.20% and 11.47% of nitrogen are found in their char, respectively. According to Sun et al. (2024), N and P can catalyse carbonisation process and interact with carbon to form a strong structure. While HS have the highest carbon content (80.26%) with less oxygen content (7.81%) compared to others, indicating HS can be a carbon source for the char residues of EPS.

Raman spectra of char residues from different samples are shown in Fig. S7. The Raman spectrum consists of two bands: the D band at 1360 cm^{-1} and the G band at 1600 cm^{-1}. The graphitisation degree is calculated as a ratio of disordered carbonaceous structure and graphitic components related to the intensity of D and G bands, respectively. The lower I_D/I_G indicates a higher graphitisation degree, microcrystalline

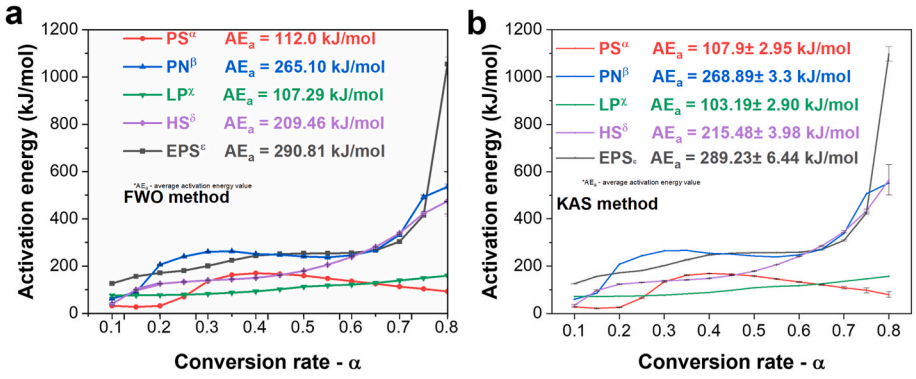

Fig. 3. Activation energy following conversion rate, and the average activation energy values of PS, PN, LP, HS, and EPS from the FWO (a), and the KAS (b) methods. The different superscript symbols imply significant difference between values ($p < 0.05$).

Table 2
Elemental contents and graphitisation degree calculated from Raman spectroscopy of char residues from EPS and their isolated components at 700 °C.

Sample	PS	PN	LP	HS	EPS
C (%)	$44.2 \pm 5.0^{\alpha}$	$73.0 \pm 0.59^{\beta}$	$74.04 \pm 1.91^{\zeta}$	$80.26 \pm 2.83\delta$ 1	$81.60 \pm 3.17\varepsilon$
O (%)	$49.72 \pm 5.61^{\alpha}$	$16.14 \pm 0.62^{\beta}$	$21.85 \pm 4.8^{\zeta}$	$7.81 \pm 0.023^{\delta}$	$10.07 \pm 1.84^{\varepsilon}$
N (%)	2.31 ± 0.26	10.20 ± 0.42	2.18 ± 0.25	11.47 ± 0.87	7.57 ± 0.55
P (%)	2.90 ± 0.32	0.56 ± 0.021	1.89 ± 0.145	0.37 ± 0.107	0.68 ± 0.36
S (%)	0.81 ± 0.09	0.07	0.04 ± 0.0003	0.09 ± 0.01	0.080 ± 0.04
Graphitisation degree (I_D/I_G)	1.35	1.31	1.39 ± 0.25	1.33	1.60

The different superscript symbols in same row imply significant difference between values ($p < 0.05$).

carbonaceous structure, and smaller porosity, which is beneficial for blocking heat transfer and releasing gaseous products. As shown in Fig. S7, the I_D/I_G ratio of the char layer from EPS and their component follows the sequence of PN (1.31) < HS (1.33) < PS (1.35) < LP (1.39) < EPS (1.60). The results demonstrate that the PN and HS can produce more graphite structure-like char residues than PS, LP, and EPS. The reason can be due to the higher aromatic structure and nitrogen content of HS and PN compared to LP and PS.

3.2.2. FTIR characterisation and PCA analysis of char residues

To investigate the relationship between the functional groups of EPS components and their char formation behaviour, as well as to elucidate their thermal degradation mechanisms, the char residues of each EPS component at various temperatures were collected from TGA testing and analysed by FTIR, as shown in Fig. 4 and Fig. S8. The wavenumbers corresponding to the functional groups of these samples are shown in Table S1. However, it is apparent that the changes in functional groups of these samples are not clear at some temperature ranges (e.g. 100-300 °C, and 600-800 °C). Therefore, in this study, the PCA are applied to monitor the changes in the FTIR spectra following the temperature of each sample. In general, the changes in FTIR spectra of each sample can be visualised by two principal components (PC), which account for more than 80% of the total variation. This implies that both the first (PC1) and the second (PC2) principal components can be used to illustrate the variation of the FTIR spectrum at different temperatures in each sample. Particularly, the total variation of the first PC (PC1) and the second PC (PC2) of EPS is the lowest (80.6%) among the samples, suggesting the complexity of their char formation process.

In the case of PS, PC1 negative loadings are associated with bands at 3500–3000 cm^{-1}, 3000–2800 cm^{-1}, and 960 cm^{-1}, corresponding to –OH groups, C–H stretching of $–CH_3$ and $–CH_2$, and P–O–C groups, respectively (Wang et al., 2018). In contrast, its positive values are correlated to the C–O–C/P–O–P vibrations at 1085–1000 cm^{-1} (Cabrera-Barjas et al., 2023). Likewise, PC2 positive loadings represent peaks at 4000–35000, 3000–2800, 1680–1450, 1350–1250, 960, and 600–900 cm^{-1}, which are attributed to –OH, C–H, C=C, C–O/C–N, P–O–C, and aromatic C–H vibrations, respectively. Negative PC2 loadings emphasise weak bands at 1085–1000 and 960 cm^{-1}. In the temperature range of 100 – 200 °C, the PC2 score remains stable, while the PC1 score becomes slightly more negative, likely due to dehydration involving –OH groups. This result is also consistent with the activation energy values, where they keep stable at $\alpha = 0.1$-0.2. As the temperature rises to 300 °C, PC1 is still in the negative region, but rockets to 1.27 at 700 °C. Meanwhile, the PC2 decreases sharply to −1.45 at 400 °C. Obviously, the changed direction to negative position in PC2, and positive position in PC1 indicates the promotion of C–O–C peak, which is related to the formation of ether in levoglucosenone – an intermediate product of cellulose (Jiang et al., 2023). In agreement with AE results, in this temperature range of 200-400 °C, the AE of PS achieve a maximum value of 170 kJ/mol (Fig. 3). In addition, this trend also underscores the role of phosphorus in catalysing carbonisation due to the presence of P-O-C in PC2's negative loading. From 400 to 700 °C, both PC1 and PC2 scores shift toward positive values. Although the positive PC1 loadings represent fewer functional groups than the negative ones, their increase correlates with the enrichment of C–O–C/P–O–P structures. PC2, which retains broader functional group representation, also increases, indicating debranched and depolymerised structure(Tao et al., 2021), leading to the char formation. At 800 °C, PC1 and PC2 scores diverge in a way of the loss of the most unstable functional groups. However, persistent signals from C–O–C/P–O–P and P–O–C groups point to the formation of a phosphorus-reinforced char structure. The char formation mechanisms of other EPS components are further discussed in Text S1.1. In general, the char formation mechanism of EPS components is primarily driven by two fundamental processes: the thermal degradation of functional groups and their subsequent recombination into more stable structures. For example, the FTIR spectrum of LP at 100 °C is characterised by negative PC1 scores, largely associated with C-H groups, reflecting their aliphatic nature. However, as the temperature rises, the aliphatic structure of LP is broken down, resulting in the formation of various functional groups. Notably, at 700–800 °C, both PC1 and PC2 scores shift positively, likely due to Diels–Alder cyclisation reactions between dienes and alkenes. This mechanism explains the slight difference in the graphitisation degree of LP compared to other EPS components (I_D/I_G = 1.31-1.39) and the small LP's residue (remaining 3.91%) until 900 °C.

3.3. Flammability behaviour

The flammability properties of EPS and their isolated component are measured using microcombustion calorimeter (MCC). The MCC results are reliable indicators of the flammability of a material, with lower values of peak heat release rate (pHRR), and the total heat release (THR) typically reflecting better flame-retardant performance (Jaouahar et al., 2025). The pHRR, the temperature of pHRR (T_{pHRR}) and THR of all samples are illustrated in Table 3.

PS have the lowest pHRR values of 29.68 W/g, followed by HS (115.03 W/g) and PN (135.38 W/g), indicating their major roles in reducing heat release rate when burning EPS – this should be related to the char formation. The pHRR value of LP is significantly higher than that of other samples due to the emission of combustible gases during their decomposition. In contrast, PS, PN, and HS primarily release non-combustible gases, which is demonstrated in the following section. A similar trend to pHRR is also observed in the THR. The THR values are 5.20 kJ/g for PS, 14.45 kJ/g for HS, and 16.27 kJ/g for PN, and 29.81 kJ/g for LP. According to Bassett et al. (2025), the THR values are closely related to the char formation and the quantity of char residues. PS have the lowest THR due to the highest char yield, while LP have the highest THR and the lowest char yield among samples. Interestingly, the pHRR of PS isolated from EPS is significantly lower than lignin (Dorez et al., 2014) and DNA (Alongi et al., 2015), comparable to phosphorated cellulose fibre (Zhang et al., 2022). Although DNA shows effective char formation, its high cost and limited availability make EPS a more practical and scalable alternative. Meanwhile, the phosphorated cellulose fibre has to be synthesised in various steps. These findings not only show the potential for flame-retardant applications of EPS themselves, but also for each EPS component. Further, the T_{pHRR} of all samples are higher than those reported for DNA (Alongi et al., 2015) and phosphorylated cellulose fibre (Zhang et al., 2022), indicating their potential suitability for flame-retardant applications, which usually require high thermal stability.

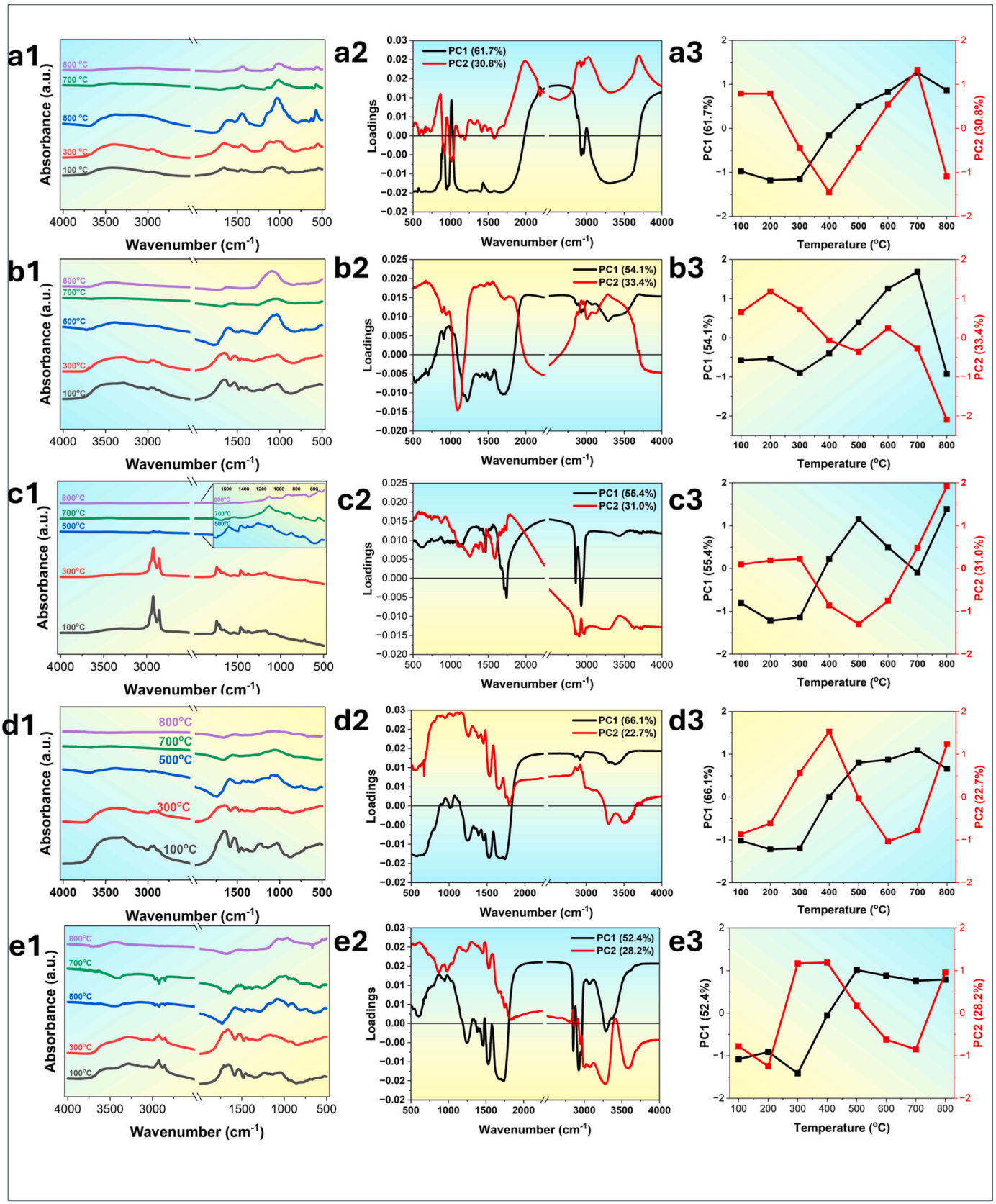

Fig. 4. FTIR spectra (a1-e1), PCA loadings (a2-e2), and PCA scores (a3-e3) of PS (a1-3), PN (b1-3), LP (c1-3), HS(d1-3), and EPS (e1-3) at different temperatures.

Table 3
MCC data of EPS and their isolated components.

Samples	pHRR (W/g)	T_{pHRR} (°C)	THR (kJ/g)	Ref.
EPS	86.49^{α}	349.84^{α}	$15.16 \pm 0.01^{\alpha}$	This study
Polysaccharides	$29.68 \pm 0.0^{3\beta}$	$323.95 \pm 1.15^{\beta}$	$5.20 \pm 0.05^{\beta}$	This study
Proteins	135.38^{ζ}	$367.29 \pm 2.07^{\zeta}$	$16.27 \pm 0.587^{\zeta}$	This study
Lipids	205.03 ± 1.43/*$164.24 \pm 1.15^{\delta}$	315.61 ± 1.46/*$395.30 \pm 1.44^{\delta}$	$29.81 \pm 10.5^{\delta}$	This study
Humic-like substances	115.03^{ε}	362.66ε	14.45^{ε}	This study
DNA	42	223	-	Alongi et al. (2015)
Phosphorated cellulose fibre	29.6	247.1	2.2	Zhang et al. (2022)
Lignin	36	350	4.5	Dorez et al. (2014)

- not available;/*a second peak.
The different superscript symbols in a same column imply significant difference between values ($p < 0.05$).

3.4. Pyrolytic gas products analysis

3.4.1. Pyrolytic gas

Combustion of materials is directly related to the fire reaction between the pyrolytic gases released and oxygen. Therefore, characterisation of the gases released during the decomposition can provide vital information for understanding the flammability of materials. In this study, the TG-FTIR method was used to identify the functional groups of the gas released during the thermal decomposition of EPS components, as shown in Fig. 5.

The characteristic peaks of the gaseous products are shown in Table S2. As shown in the 3D graph, the gases released from EPS cover all functional groups in their components. No prominent peaks appeared before 200 °C, indicating the volatilisation occurred from this temperature. From 200 to 600 °C, the CO_2 (peak at 2363 cm^{-1}) displays the highest absorption peaks in the spectrum of PS, PN, and HS, indicating that carboxylation is the primary reaction in the degradation of these components. CH_4 (peak at 2930 cm^{-1}) is the main pyrolysis product of LP, consistent with its aliphatic-rich structure. In addition, T_{pHRR} values observed in the MCC results closely correspond to the peak release temperatures of specific gases—CO_2 for PS, PN, and HS; CH_4 for LP; and both CO_2 and CH_4 for EPS—suggesting that these gases are the primary contributors to heat release during the combustion of each component. As shown in Fig. 5f, the gaseous products of EPS mainly consist of CO_2 (39.47 %) and CH_4 (25.70 %), accounting for over 50% of the total gas emissions, which highlights the dominant role of these gases in the combustion process. In addition, along with CO_2, the gas phase of PN also contains the highest N-containing compound content of 24.46 %, followed by HS with 19.94%. CO_2 and NH_3 are non-combustible gases that dilute oxygen concentration, reducing fire propagation. CH_4 is a hydrocarbon that can facilitate fire, which is not advantageous for flame-retardant applications. These findings indicate the higher flammability of LP relative to the other EPS components.

3.4.2. Functional group evolution in gas phase

To better understand the gaseous release mechanism from EPS and their components, the 2D-COS analysis is applied. In the 2D-COS

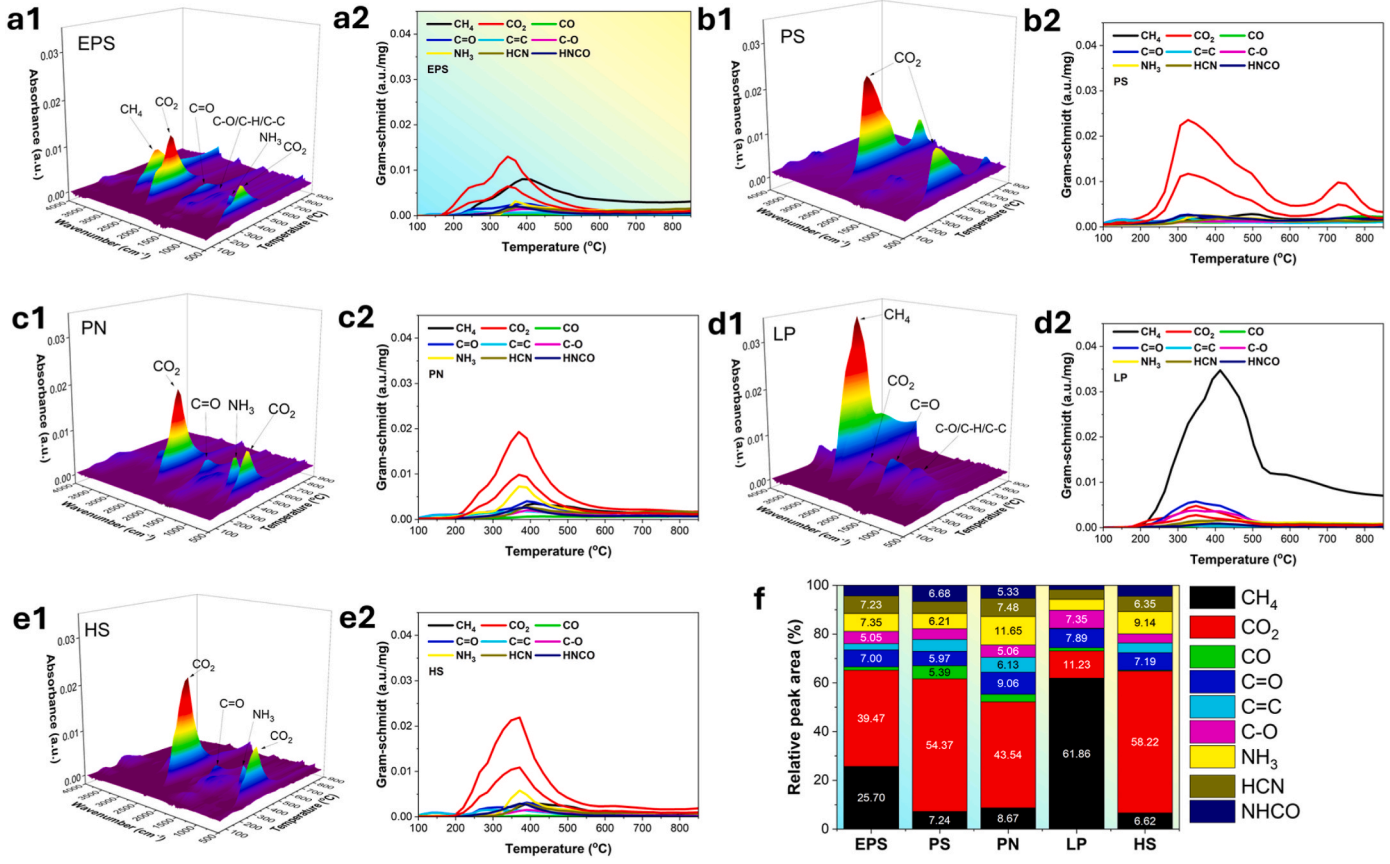

Fig. 5. 3D FTIR spectra and changes of specific gas absorption peak following temperature from PS (a1-2), PN (b1-2), LP (c1-2), HS (d1-2), and EPS (e1-2) and their relative peak area of the gaseous product (f).

synchronous map shown in Fig. 6, the auto-peaks in the diagonal position point out the functional groups susceptible to temperature. The significant auto-peak is observed at wave numbers of 2363 cm^{-1}, which is attributed to the CO_2 in synchronous maps of PS, PN, and HS. This suggests that the primary reaction mechanism of these compounds is decarboxylation. In the case of LP, the significant auto-peak appears at the peak of 2930 cm^{-1} due to the release of CH_4, which is one of major gases from the demethylation or cracking of the aliphatic structure of LP. As a result, the synchronous spectra of EPS show two significant auto-peaks at 2363 cm^{-1} and 2930 cm^{-1}, indicating the significant effects of LP on the gas release of EPS. As mentioned, the release of CO_2 contributes to fire suppression by diluting oxygen and absorbing heat. Meanwhile, CH_4, mainly released by LP, can facilitate the fire reaction. In addition, several autocorrelation peaks found from 1900 to 600 cm^{-1} underscore the complexity of the pyrolysis process. For example, in the synchronous 2D correlation map of PS, cross-peaks $\phi(x_1, x_2)$ are observed at (2363 cm^{-1}, 3736 cm^{-1}), (2363 cm^{-1}, 2930 cm^{-1}), (2363 cm^{-1}, 1722 cm^{-1}), and (2363 cm^{-1}, 1463 cm^{-1}), corresponding to CO_2 and the functional groups OH/CH_4, C=O of ketones, carboxylic groups, and C=C of aromatics, respectively. These cross-peaks indicate that the thermal variations of these functional groups follow a similar trend to that of CO_2. In contrast, cross-peaks between CO_2 and N-containing bands are weak, likely due to the low nitrogen content in PS.

In 2D-COS, the asynchronous signals (Fig. S9) indicate the sequential changes of functional groups by the temperature. In the asynchronous map of PS, CO_2 also creates various positive cross peaks with other gases Ψ (2363 cm^{-1}, 2930/1722/1463/1175/965/715/2281 cm^{-1}), except that Ψ(2363 cm^{-1}, 3736 cm^{-1}) is negative, indicating CO_2 release after H_2O, phenols, alcohols, but before all of gases, following Noda's rule (Lasch and Noda, 2019). The thermal decomposition of PS starts with the release of H_2O, phenols, alcohols and CO_2 due to the dehydration and decarboxylation reaction, which breaks the 1,4-glucosidic bond and the ring-opening in the PS structure (Cabrera-Barjas et al., 2023). The results of sequential changes in the functional groups of PS are shown in Table S3 and Fig. 7. The changes of PS are in order of H_2O, phenols, alcohols → CO_2 → NHCO → Ketones, carboxylic acids, aldehydes, amides → Aromatics → NH_3 → HCN → CH_4 → Phenols, ethers, alcohols → CO. The release of NHCO groups in the gas phase can be the result of dehydration under the catalyst of phosphorus species, decarboxylation, and retro Diels-Alder reaction, as reported by Cabrere-Barjas et al. (Cabrera-Barjas et al., 2023). The release of other gases can result from multiple reaction pathways, as shown in Fig. S10. For example, the formation of ketones, aldehydes, and amides may be due to the decarboxylation and deoxygenation reaction with olefin as a by-product. The olefins can be converted to aromatic products through Diels-Alder, cyclisation, cracking and many other reactions (Yang et al., 2019). The sequential changes in functional groups of other components are discussed in detail in Text S1.2 and shown in Fig. 7. As can be seen, the sequences of PS, PN and HS begin with a band of 4000 – 3500 cm^{-1} due to the release of water, phenols, and alcohols, followed by the decarboxylation process, as demonstrated by the release of CO_2. The earlier release of CO_2 and H_2O is beneficial for quickly reducing the oxygen supplied to the fire. Afterwards, they start releasing various gaseous products, such as ketones, carboxylic acids, aldehydes (C=O), aromatic (C=C), NH_3, and HCN, due to cracking, deamination, dehydration, decarboxylation, and deoxygenation reactions.

For LP, volatile compounds evolve before methane formation (from 250 °C), including low-molecular-mass, readily combustible compounds, such as phenols, ketones, aldehydes, aromatics, and short-chain fatty acids. In other words, LP is prone to ignition and efficient combustion at lower temperatures (<250 °C) because it can be transformed to combustible gases more easily. Notably, the sequence of LP's gaseous products is CO → NH_3, indicating the decarbonylation and deamination process of char structure, resulting in the loss of most functional groups in LP char. In the anaerobic pyrolysis, the presence of CO can also represent the Boudouard reaction (C + CO_2 → CO) occurring at 250 – 700 °C, suggesting the degradation of char products (Chen et al., 2020b). Although the Boudouard reaction is not beneficial for the amount of char residues, the CO from this reaction and NH_3 are non-combustible, which could dilute the oxygen concentration for fire. The position of CO appears at the end of the sequences of EPS, PS, and PN, implying that its evolution requires higher energy and reflects the greater stability of their char residues.

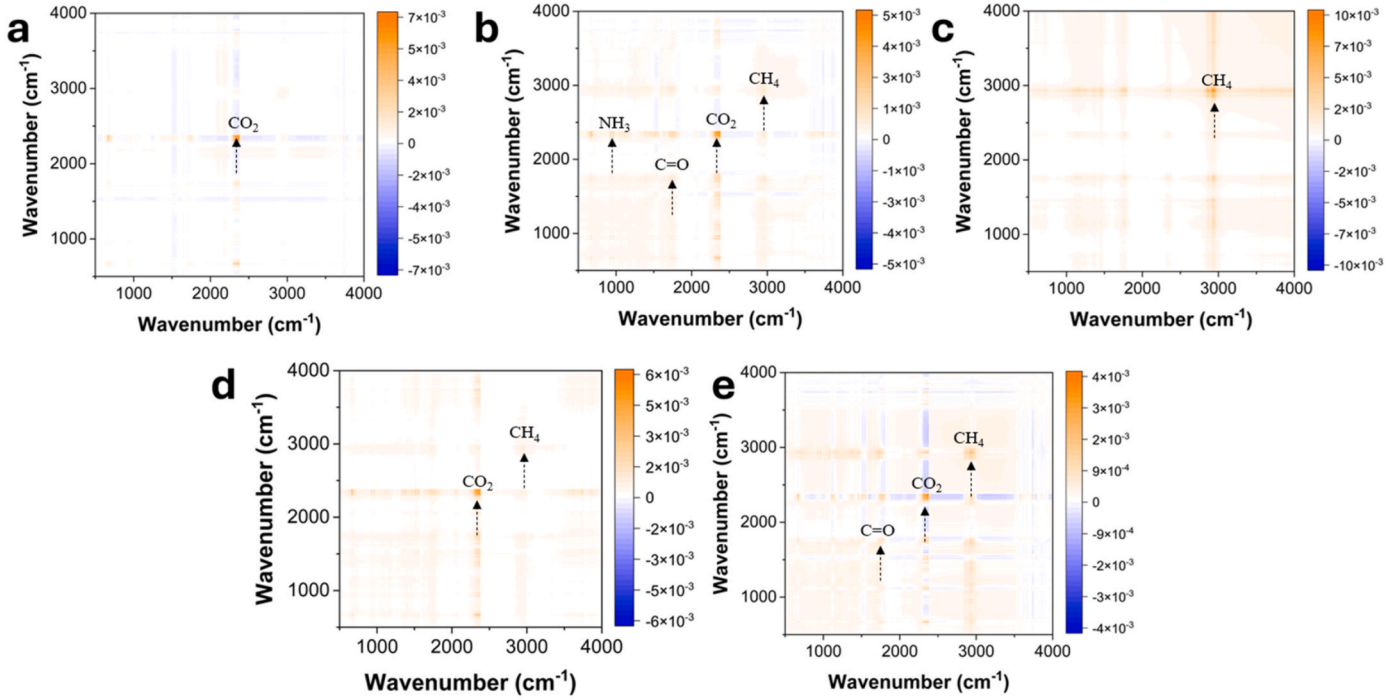

Fig. 6. 2D COS synchronous spectra of PS (a), PN (b), LP (c), HS (d), and EPS (e).

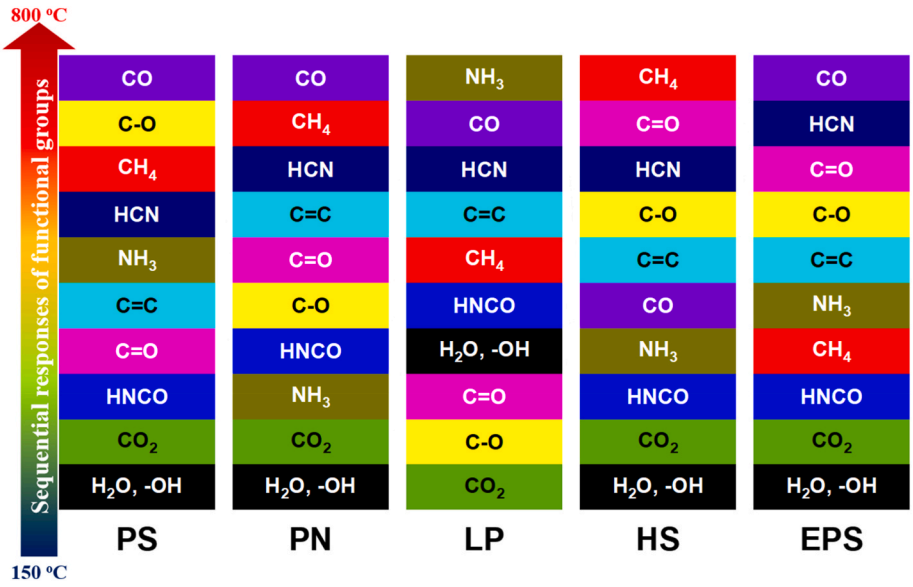

Fig. 7. Sequential changes in functional groups in the gas phase of PS, PN, LP, HS and EPS.

3.5. Future perspectives

According to Zheng et al. (2024), the economic value of EPS is estimated to be 10 – 20 times higher than that of biogas produced from an equivalent amount of organic carbon. In the Netherlands, the production of EPS can bring approximately 170 million euros for ten WWTPs by 2030 (van Leeuwen et al., 2018). With the enormous amount of municipal sludge all over the world, the production of EPS is expected to create a new value chain for WWTPs following the circular economy. Meanwhile, the flame-retardant market is forecasted to reach 9.5 billion US dollars by 2027, offering a significant opportunity for the use of EP (Holguin, 2024). However, the EPS composition could be affected by many environmental and operational parameters, resulting in a critical barrier to developing consistent and reliable EPS-based flame retardants. Therefore, understanding the properties of EPS is an essential step for developing further applications since they are still considered "secret" materials (Seviour et al., 2019). In this study, we observed that PS plays a significant role in reducing the heat release rate, and PN and HS contribute to the thermal properties and char structure of EPS. LP shows a more negative influence on EPS's thermal and flame-retardant properties due to its higher flammability and lower char yield. Interestingly, our analysis of gas and condensed phases suggests that the interaction among these components within EPS can reduce gas release and enhance thermal properties when compared to the individual compounds. Therefore, further investigation into the interactions, particularly the role of LP, is necessary to better understand and optimise the EPS structure for flame-retardant applications. This study also proposes a novel strategy to control the properties of EPS by tuning their composition. This strategy enables targeted formulation of EPS with optimised thermal and flame-retardant properties, while reducing compositional variability across sludge sources. In addition, isolated components also have their own application; for example, LP could be used to produce biofuel (Khalil et al., 2025). In the future, the optimal EPS composition by mixing these components for flame retardant application should be evaluated in detail. The extra advantage of developing an optimal blend of the components of EPS should be balanced to the likely extra production costs of optimising the blend.

4. Conclusions

The thermal and flammability properties of EPS components were analysed to provide insight into their flame-retardant mechanisms. Polysaccharides extracted from EPS exhibited the lowest peak heat release rate and total heat release of 29.7 W/g and 5.20 kJ/g, respectively, and the highest char residue of 48.7% at 900 °C, indicating strong flame-retardant potential. Protein and humic-like substances had the higher activation energy than other components and formed more graphite-like char as an effective protective barrier against heat transfer and volatile release during combustion. Polysaccharides, proteins and humic-like substances generate non-combustible gases that suppress fire propagation. In contrast, lipids showed lower thermal stability, produced minimal char, and released combustible gases, such as CH_4, which potentially impairs the flame-retardant properties of EPS. Lipids might exhibit synergistic effects within the EPS, potentially enhancing EPS overall thermal performance. This study reveals that the flame-retardant performance of EPS does not arise from a single dominant component alone, but from the complementary contributions of polysaccharides, proteins, and humic-like substances in both the condensed and gas phases. Further research is needed to optimise the interactions between lipids and other components to enhance EPS flame-retardant efficiency. Moreover, by optimising extraction parameters to mitigate the pro-flammability of lipid fractions and maximise the yield of components with high charring capacity and non-combustible gas release, it is possible to produce tailored flame-retardant additives. Such developments would not only enhance the fire safety of polymer composites but also contribute to the circular economy by repurposing biological waste into functional materials.

CRediT authorship contribution statement

Tan Minh Le: Conceptualization, Formal analysis, Investigation, Methodology, Visualization, Writing – original draft, Writing – review & editing. **Yuemei Lin:** Conceptualization, Methodology, Supervision, Writing – review & editing. **Wei-Qin Zhuang:** Methodology, Writing – review & editing. **Krishnan Jayaraman:** Conceptualization, Investigation, Methodology, Supervision, Writing – review & editing. **Nam Kyeun Kim:** Conceptualization, Funding acquisition, Investigation, Methodology, Project administration, Supervision, Writing – review & editing.

Declaration of competing interest

The authors declare that they have no known competing financial interests or personal relationships that could have appeared to influence

the work reported in this paper.

Acknowledgements

This research is supported by the Marsden Fast-Start Fund (Grant number: MFP-UOA2218) from Royal Society Te Apārangi (New Zealand). We acknowledge the sourcing of materials from Ms. Yan Sun, and Mr. Rob Tinholt, Watercare Services Limited in Auckland, New Zealand. The authors would like to thank Dr. Cheng Wang and Prof. Guan Heng Yeoh from the School of Mechanical and Manufacturing Engineering, the University of New South Wales, Australia for supporting the TG-FTIR measurement.

Appendix A. Supplementary data

Supplementary data to this article can be found online at https://doi.org/10.1016/j.jclepro.2026.148694.

Data availability

Data will be made available on request.

References

Aiken, G.R., Mcknight, D.M., Wershaw, R.L., Maccarthy, P., 1986. Humic substances in soil, sediment, and water. 1985. Soil Sci. 142, 323.
Alongi, J., Di Blasio, A., Milnes, J., Malucelli, G., Bourbigot, S., Kandola, B., Camino, G., 2015. Thermal degradation of DNA, an all-in-one natural intumescent flame retardant. Polym. Degrad. Stabil. 113, 110–118.
Anca-Couce, A., 2016. Reaction mechanisms and multi-scale modelling of lignocellulosic biomass pyrolysis. Prog. Energy Combust. Sci. 53, 41–79.
Antunes, E.C., Cintra, B., Bredel, M., Temmink, H., Schuur, B., 2024. Fractionation of extracellular polymeric substances by aqueous three-phase partitioning systems. Ind. Eng. Chem. Res. 63, 10748–10760.
Bassett, A.H., Morgan, A.B., Palmese, G.R., 2025. Investigating the effects of furan ring substitution and network position on char formation in intrinsically flame-retardant epoxy resins. Polym. Degrad. Stabil. 241, 111538. https://doi.org/10.1016/J.POLYMDEGRADSTAB.2025.111538.
Cabrera-Barjas, G., Jimenez, R., Romero, R., Valdes, O., Nesic, A., Hernández-García, R., Neira, A., Alejandro-Martín, S., de la Torre, A.F., 2023. Value-added long-chain aliphatic compounds obtained through pyrolysis of phosphorylated chitin. Int. J. Biol. Macromol. 238, 124130.
Chen, J., Zhang, J., Liu, J., He, Y., Evrendilek, F., Buyukada, M., Xie, W., Sun, S., 2020b. Co-pyrolytic mechanisms, kinetics, emissions and products of biomass and sewage sludge in N2, CO2 and mixed atmospheres. Chem. Eng. J. 397, 125372.
Chen, W.-H., Eng, C.F., Lin, Y.-Y., Bach, Q.-V., 2020a. Independent parallel pyrolysis kinetics of cellulose, hemicelluloses and lignin at various heating rates analyzed by evolutionary computation. Energy Convers. Manag. 221, 113165.
Dai, X., Luo, F., Dai, L., Dong, B., 2013. Degradation of extracellular polymeric substances (EPS) in anaerobic digestion of dewatered sludge. Procedia Environ. Sci. 18, 515–521.
Dorez, G., Ferry, L., Sonnier, R., Taguet, A., Lopez-Cuesta, J.-M., 2014. Effect of cellulose, hemicellulose and lignin contents on pyrolysis and combustion of natural fibers. J. Anal. Appl. Pyrolysis 107, 323–331.
Enescu, D., Frache, A., Lavaselli, M., Monticelli, O., Marino, F., 2013. Novel phosphorous–nitrogen intumescent flame retardant system. Its effects on flame retardancy and thermal properties of polypropylene. Polym. Degrad. Stabil. 98, 297–305.
Hamed, H. Ben, Mainardis, M., Moretti, A., Toye, D., Léonard, A., 2025. Extracellular polymeric substances (EPS) in sewage sludge management: a call for methodological standardization. J. Environ. Manag. 376, 124407.
Holguin, M., 2024. Global flame retardants market dynamics and trends. Plast. Eng. 2–4.
Jaouahar, M., Ablouh, E.-H., Hanani, Z., Humar, M., El Achaby, M., Sehaqui, H., 2025. Comprehensive characterization of hygroscopic, fire-retardant and thermally insulating sulfated nanocellulose aerogel. Chem. Eng. J., 160236
Jeong, S.H., Park, C.H., Song, H., Heo, J.H., Lee, J.H., 2022. Biomolecules as green flame retardants: recent progress, challenges, and opportunities. J. Clean. Prod., 133241
Jiang, Y., Li, C., Hou, Z., Shi, X., Zhang, X., Gao, Y., Deng, S.-H., 2023. Pollutants removal and connections among sludge properties, metabolism potential and microbial characteristics in aerobic granular sequencing batch reactor for petrochemical wastewater treatment. J. Environ. Manag. 344, 118715.
Khalil, N.A., Banjar, M.F., Abedin, F.N.J., Fizal, A.N.S., Ahmad, N., Zulkifli, M., Taweepreda, W., Hossain, M.S., Ahmad Yahaya, A.N., 2025. Potential of lipids from polymer-based dewatered sewage sludge as feedstock for biodiesel production. Sustainability 17, 2991.
Kim, N.K., Bhattacharyya, D., van Loosdrecht, M., Lin, Y., 2023. Enhancement of fire resistance and mechanical performance of polypropylene composites containing cellulose fibres and extracellular biopolymers from wastewater sludge. Polym. Test. 127, 108185.
Kim, N.K., Lin, R., Bhattacharyya, D., van Loosdrecht, M.C.M., Lin, Y., 2022. Insight on how biopolymers recovered from aerobic granular wastewater sludge can reduce the flammability of synthetic polymers. Sci. Total Environ. 805, 150434.
Kim, N.K., Mao, N., Lin, R., Bhattacharyya, D., van Loosdrecht, M.C.M., Lin, Y., 2020. Flame retardant property of flax fabrics coated by extracellular polymeric substances recovered from both activated sludge and aerobic granular sludge. Water Res. 170, 115344.
Lasch, P., Noda, I., 2019. Two-dimensional correlation spectroscopy (2D-COS) for analysis of spatially resolved vibrational spectra. Appl. Spectrosc. 73, 359–379.
Le, T.M., Lin, Y., Zhuang, W.-Q., Jayaraman, K., Kim, N.K., 2025. Effects of extraction methods on the thermal stability of extracellular polymeric substances-based biomaterials from wastewater sludge. Environ. Sci. Technol. https://doi.org/10.1021/acs.est.4c10329.
Lee, H., Kim, N.K., Verbeek, C.J.R., Bhattacharyya, D., 2024. A novel approach utilising phosphorylated casein for fire-retardant and formaldehyde-free medium density wood fibreboards. Ind. Crops Prod. 215, 118608.
Li, C., Liu, J., Yu, C., Lou, G., 2024. Feasibility analysis of continuous extraction of biomaterials from flocculant sludge and potential applications in the fire protection field. J. Environ. Manag. 370, 122351.
Li, J., Hao, X., Persiani, R., van Loosdrecht, M.C.M., Lin, Y., 2024. Reinvestigating the composition of alginate-like exopolymers extracted from activated sludge. ACS ES&T Water 4, 3007–3015.
Liu, C., Li, P., Xu, Y., Liu, Y., Zhu, P., 2023. Synergistic effects of iron alginate on improving the fire safety and mechanical properties of epoxy resin/ammonium polyphosphate composites. Macromol. Mater. Eng. 308, 2200516.
Liu, H.-M., Yao, Y.-G., Yan, Y.-Y., Wang, X.-D., 2020. Elucidation of the structural changes of sesame hull hemicelluloses during roasting. Int. J. Biol. Macromol. 161, 1535–1544.
Michalska, J., Turek-Szytow, J., Dudło, A., Surmacz-Górska, J., 2022. Characterization of humic substances recovered from the sewage sludge and validity of their removal from this waste. EFB Bioeconomy J. 2, 100026.
Minh Le, T., Lin, Y., Zhuang, W.-Q., van Loosdrecht, M.C.M., Jayaraman, K., Kim, N.K., 2025. Unlocking the potential flame-retardant mechanisms of extracellular polymeric substances recovered from municipal sludge. J. Environ. Chem. Eng., 117907 https://doi.org/10.1016/J.JECE.2025.117907.
Noda, I., Dowrey, A.E., Marcott, C., Story, G.M., Ozaki, Y., 2000. Generalized two-dimensional correlation spectroscopy. Appl. Spectrosc. 54, 236A–248A.
Qiu, C., Chen, Z., Hu, F., Wu, H., Wang, L., Liu, M., Zhou, K., 2024. Simultaneous extraction of oil, protein and polysaccharide from residual seed cake of Camellia oleifera Abel. using three phase partitioning. Ind. Crops Prod. 209, 117994.
Schinazi, G., Price, E.J., Schiraldi, D.A., 2022. Fire testing methods of bio-based flame-retardant polymeric materials. In: Bio-Based Flame-Retardant Technology for Polymeric Materials. Elsevier, pp. 61–95.
Seviour, T., Derlon, N., Dueholm, M.S., Flemming, H.-C., Girbal-Neuhauser, E., Horn, H., Kjelleberg, S., Van Loosdrecht, M.C.M., Lotti, T., Malpei, M.F., 2019. Extracellular polymeric substances of biofilms: suffering from an identity crisis. Water Res. 151, 1–7.
Stefanidis, S.D., Kalogiannis, K.G., Iliopoulou, E.F., Michailof, C.M., Pilavachi, P.A., Lappas, A.A., 2014. A study of lignocellulosic biomass pyrolysis via the pyrolysis of cellulose, hemicellulose and lignin. J. Anal. Appl. Pyrolysis 105, 143–150.
Sun, L., Ding, L., Guo, X., Wang, Y., Liu, X., Ren, Y., Li, Y., 2024. “One for two” strategy to construct an organic-inorganic polymer colloid for flame-retardant modification of flax fabric and rigid polyurethane foam. Int. J. Biol. Macromol. 275, 133562.
Tain, Y.-L., Chang, S.K.C., Liao, J.-X., Chen, Y.-W., Huang, H.-T., Li, Y.-L., Hou, C.-Y., 2021. Synthesis of short-chain-fatty-acid resveratrol esters and their antioxidant properties. Antioxidants 10, 420.
Tang, Y., Dai, X., Dong, B., Guo, Y., Dai, L., 2020. Humification in extracellular polymeric substances (EPS) dominates methane release and EPS reconstruction during the sludge stabilization of high-solid anaerobic digestion. Water Res. 175, 115686.
Tao, W., Zhang, P., Yang, X., Li, H., Liu, Y., Pan, B., 2021. An integrated study on the pyrolysis mecanism of peanut shell based on the kinetic analysis and solid/gas characterization. Bioresour. Technol. 329, 124860.
van Leeuwen, K., de Vries, E., Koop, S., Roest, K., 2018. The energy & raw materials factory: role and potential contribution to the circular economy of the Netherlands. Environ. Manag. 61, 786–795.
Venezia, V., Portarapillo, M., De Falco, G., Sanchirico, R., Luciani, G., Di Benedetto, A., 2023. Humic acids on fire? physico-chemical, thermal, flammability features and extraction process of different humic acids in support of their possible applications. Chemosphere 344, 140430.
Wang, C., Wu, Y., Li, Y., Shao, Q., Yan, X., et al., 2018. Flame-retardant rigid polyurethane foam with a phosphorus-nitrogen single intumescent flame retardant. Polym. Adv. Technol. 29, 668–676. https://doi.org/10.1002/pat.4105.
Wang, X., Tang, X., Yang, X., 2017. Pyrolysis mechanism of microalgae nannochloropsis sp. based on model compounds and their interaction. Energy Convers. Manag. 140, 203–210.
Wei, L., Li, J., Xue, M., Wang, S., Li, Q., Qin, K., Jiang, J., Ding, J., Zhao, Q., 2019. Adsorption behaviors of Cu2+, Zn2+ and Cd2+ onto proteins, humic acid, and polysaccharides extracted from sludge EPS: sorption properties and mechanisms. Bioresour. Technol. 291, 121868.
Yang, C., Li, R., Zhang, B., Qiu, Q., Wang, B., Yang, H., Ding, Y., Wang, C., 2019. Pyrolysis of microalgae: a critical review. Fuel Process. Technol. 186, 53–72.
Yu, J., Xiao, K., Xu, H., Li, Y., Xue, Q., Xue, W., Zhang, A., Wen, X., Xu, G., Huang, X., 2023. Spectroscopic fingerprints profiling the polysaccharide/protein/humic architecture of stratified extracellular polymeric substances (EPS) in activated sludge. Water Res. 235, 119866. https://doi.org/10.1016/J.WATRES.2023.119866.

Yu, W., Wen, Q., Yang, J., Xiao, K., Zhu, Y., Tao, S., Liang, S., Hu, S., Wu, Q., Hou, H., 2020. Novel insights into extracellular polymeric substance degradation, hydrophilic/hydrophobic characteristics, and dewaterability of waste activated sludge pretreated by hydroxylamine enhanced fenton oxidation. Acs Es&T Eng 1, 385–392.

Yuan, Z., Luo, J., Ndudi, E.A., Ma, W., Zhu, N., Lou, Z., 2022. Systematic understanding of char-volatile evolution and interaction mechanism during sewage sludge pyrolysis through in-situ tracking solid-state reaction and products fate. J. Hazard Mater. 432, 128669.

Zhang, C., Chao, L., Zhang, Z., Zhang, L., Li, Q., Fan, H., Zhang, S., Liu, Q., Qiao, Y., Tian, Y., 2021. Pyrolysis of cellulose: evolution of functionalities and structure of bio-char versus temperature. Renew. Sustain. Energy Rev. 135, 110416.

Zhang, Q., Liu, X., Ren, Y., Li, Y., 2022. Phosphorated cellulose as a cellulose-based filler for developing continuous fire resistant lyocell fibers. J. Clean. Prod. 368, 133242.

Zhao, B., Wang, X., Yang, X., 2015. Co-pyrolysis characteristics of microalgae isochrysis and chlorella: kinetics, biocrude yield and interaction. Bioresour. Technol. 198, 332–339. https://doi.org/10.1016/j.biortech.2015.09.021.

Zheng, M., Hu, Z., Liu, T., Sperandio, M., Volcke, E.I.P., Wang, Z., Hao, X., Duan, H., Vlaeminck, S.E., Xu, K., 2024. Pathways to advanced resource recovery from sewage. Nat. Sustain. 1–10.

Zong, P., Jiang, Y., Tian, Y., Li, J., Yuan, M., Ji, Y., Chen, M., Li, D., Qiao, Y., 2020. Pyrolysis behavior and product distributions of biomass six group components: starch, cellulose, hemicellulose, lignin, protein and oil. Energy Convers. Manag. 216, 112777.